Structure of PlcR: Insights into virulence regulation and evolution of quorum sensing in Gram-positive bacteria

Nathalie Declerck*, Laurent Bouillaut†, Denis Chaix*, Nathalie Rugani*, Leyla Slamti†‡, François Hoh*, Didier Lereclus†§, and Stefan T. Arold*§

*Institut National de la Santé et de la Recherche Médicale, Unité 554, and Centre National de la Recherche Scientifique, Unité Mixte de Recherche 5048, Centre de Biochimie Structurale, Université de Montpellier, 34090 Montpellier, France; and †Unité Génétique Microbienne et Environnement, Institut National de la Recherche Agronomique, Domaine de la Minière, F78285 Guyancourt, France

Edited by Axel T. Brunger, Stanford University, Stanford, CA, and approved September 27, 2007 (received for review May 14, 2007)

Gram-positive bacteria use a wealth of extracellular signaling peptides, so-called autoinducers, to regulate gene expression according to population densities. These "quorum sensing" systems control vital processes such as virulence, sporulation, and gene transfer. Using x-ray analysis, we determined the structure of PlcR, the major virulence regulator of the *Bacillus cereus* group, and obtained mechanistic insights into the effects of autoinducer binding. Our structural and phylogenetic analysis further suggests that all of those quorum sensors that bind directly to their autoinducer peptide derive from a common ancestor and form a single family (the RNPP family, for Rap/NprR/PlcR/PrgX) with conserved features. As a consequence, fundamentally different processes in different bacterial genera appear regulated by essentially the same autoinducer recognition mechanism. Our results shed light on virulence control by PlcR and elucidate origin and evolution of multicellular behavior in bacteria.

crystal structure | tetratricopeptide repeats | transcription factor

Bacteria coordinate essential processes such as virulence, sporulation, genetic transfer, and production of antibiotics through "quorum sensing," i.e., the regulation of gene expression according to population densities. This allows coordination of the behavior of a whole community and might have been one of the early steps in the development of multicellularity (1, 2). Quorum sensing usually involves the secretion of a biomolecule, also termed "autoinducer," which is recognized by the responder cell. Gram-negative bacteria generally use systems based on secretion and recognition of acyl-homoserine lactones, whereas quorum sensing in Gram-positive species dominantly relies on the recognition of oligopeptides. These peptides elicit a response either indirectly, by triggering a two-component phosphorelay, or directly, by binding to the effector protein in the responder cell (1, 3).

PlcR is the major virulence regulator of the *Bacillus cereus* group (4). In addition to *B. cereus sensu stricto*, an opportunistic pathogen causing gastroenteritis, pneumonia, and endophthalmitis, this group includes *Bacillus thuringiensis*, an entomopathogenic bacterium used to produce biopesticides, and *Bacillus anthracis*, the causing agent of anthrax (5–7). The activity of PlcR depends on PapR, a secreted signaling peptide reimported into the bacterial cell through the Opp system (8). When high bacterial densities are reached, PapR concentrations increase inside the bacterial cells, promoting its interaction with PlcR. The PapR:PlcR complex then binds to its DNA recognition site, the palindromic PlcR box, triggering a positive feedback loop that up-regulates the expression of *plcR*, *papR*, and various virulence factors (8). The molecular basis for transcription control by PapR:PlcR is unknown.

Results

Crystal Structure of PapR-Bound PlcR. We have determined the 2.6-Å crystal structure of the complex formed between PlcR and the C-terminal PapR pentapeptide LPFEF (PapR5), both from *B. thuringiensis* strain 407 (8) (Table 1). Because PapR5 activates PlcR *in vivo* (8), the crystal structure of the complex is expected to present PlcR in its active, DNA-binding conformation.

The 34-kDa PlcR protein contains an N-terminal helix–turn–helix (HTH) DNA binding domain and a C-terminal regulatory domain, composed of 11 helices, forming five tetratricopeptide repeats (TPR) and a capping C-terminal helix [Fig. 1 and supporting information (SI) Fig. 5]. The HTH domain is directly attached to the 40-Å first TPR helix (residues 60–89; hereafter termed linker helix). Both HTH domains have motional freedom as indicated by high B-factors [a mean of 124 Å^2 as compared with 65 Å^2 for the TPR domain, when refined without translation liberation screw-motion (TLS)] and poorly defined electron density. The two PlcR molecules of the asymmetric unit dimerize via their TPR domains, burying 2,460 Å^2 of solvent-accessible surface. Intriguingly, the DNA-binding surfaces of both HTH domains of the dimer face opposite directions (Fig. 1), incompatible with their simultaneous association with the palindromic PlcR box. The absence of crystal contacts for both HTH domains supports that this potentially inactive conformation is not a crystal artifact.

Electron density corresponding to PapR5 was present in both TPR domains. The FEF motif of PapR5 binds to the concave side of the TPR domain, mainly interacting with helices 5 and 7 of the TPR domain (Fig. 1). The peptide main chain is fixed by hydrogen bonds from N159, N201, and K204. Both PapR phenylalanines insert into a hydrophobic cleft between helices 5 and 7. The PapR glutamic acid binds to Y275 of the C-terminal TPR helix and to K89, situated at the C terminus of the linker helix (Fig. 1). K197 interacts with the PapR C terminus. The C-terminal TPR helix appears relatively mobile (mean B-factor = 93 Å^2), suggesting that its position might be influenced by the peptide.

PlcR Is Structurally and Evolutionarily Related to *Enterococcus faecalis* PrgX. The structure of PlcR is strikingly similar to the structure of the sex pheromone receptor PrgX of *E. faecalis*, the only other oligopeptide quorum sensor of Gram-positive bacteria described on a molecular level (Protein Data Bank entries 2AXU and

Author contributions: N.D. and S.T.A. designed research; N.D., L.B., D.C., N.R., F.H., and S.T.A. performed research; L.B. and L.S. contributed new reagents/analytic tools; N.D., L.B., D.L., and S.T.A. analyzed data; and S.T.A. wrote the paper.

The authors declare no conflict of interest.

This article is a PNAS Direct Submission.

Abbreviations: HTH, helix–turn–helix; TPR, tetratricopeptide repeat; SAXS, small angle x-ray scattering; Rg, radius of gyration; Dm, maximum diameter.

Data deposition: The atomic coordinates and structure factors have been deposited in the Protein Data Bank, www.pdb.org (PDB ID code 2QFC).

‡Present address: M. K. Waldor Laboratory, 181 Longwood Avenue, Boston, MA 02115.

§To whom correspondence may be addressed. E-mail: didier.lereclus@jouy.inra.fr or stefan.arold@cbs.cnrs.fr.

This article contains supporting information online at www.pnas.org/cgi/content/full/0704501104/DC1.

Table 1. Data collection, phasing, and refinement statistics

	Native	SeMet
Data collection		
Space group	$P6_1$	$P6_1$
Cell dimensions		
a, *b*, *c*, Å	85.68, 85.68, 189.87	85.78, 85.78, 190.56
a, *b*, *g*, °	90.0, 90.0, 120.0	90.0, 90.0, 120.0
Wavelength, Å	0.976	0.979
Resolution, Å	2.6	3.0
R_{merge}	0.078 (0.457)	0.12 (0.41)
$I/\sigma I$	17.2 (3.2)	16.7 (5.5)
Completeness, %	100 (100)	100 (100)
Redundancy, %	8.2 (5.2)	8.4 (8.0)
Refinement		
Resolution, Å	2.6	
No. of reflections	24,200	
R_{work}/R_{free}	0.23 (0.26)/0.31 (0.39)	
rmsd		
Bond lengths, Å	0.018	
Bond angles, °	1.7	

Values in parentheses correspond to the last resolution shell.

2AXZ) (Fig. 1) (9). This resemblance is completely unanticipated, because PlcR and PrgX control different processes in different bacterial orders. Moreover, the PrgX regulatory domain lacks evident sequence similarity to PlcR and is not recognized as TPR [using TPRpred (10)]. Nonetheless the structural similarities between PlcR and PrgX are remarkable: Both are dimeric and combine a homologous HTH domain with a structurally very comparable 11-helix regulatory domain [Dali Z score (11) was 10.5 for 192 superimposed residues]. The heptapeptide pheromone cCf10 (LVTLVFV) binds PrgX in the same position and orientation as revealed for PapR:PlcR. In both PlcR and PrgX helices 5 and 7 of the regulatory domain form hydrogen bonds with the ligand backbone via asparagines and establish similar hydrophobic interactions with ligand side chains (Fig. 1). These striking resemblances strongly suggested that PlcR and PrgX diverged from the same ancestor. This was corroborated by a homology search with Psi-Blast (12): Using PrgX as bait, PlcR was retrieved with fewer than six iterations in the default setting, the commonly accepted criterion for homology (for details see *SI Text*).

Effect of PapR Binding to PlcR. We next addressed how ligand recognition regulates PlcR. In PrgX, which is constitutively associated with DNA, the HTH domains are constantly positioned in a DNA-binding orientation (Fig. 1). Apo-PrgX tetramerizes through a secondary dimerization site, formed by a C-terminal extension, leading to DNA looping and gene repression. Pheromone recognition rearranges the PrgX C-terminal extension to cover the peptide. This disrupts the secondary dimerization site, and hence DNA-looping, allowing gene transcription (9).

Conversely, PlcR binds DNA only in presence of PapR and lacks the C-terminal extension necessary for tetramerization and DNA looping. Because all of our apo-PlcR crystals failed to diffract x-rays, we used small angle x-ray scattering (SAXS) to investigate the structure of apo-PlcR. SAXS patterns of apo-PlcR recorded at 1.2–3.6 mg/ml superimposed well, implying that the overall shape or oligomerization state of apo-PlcR did not change within the concentration range tested (at higher con-

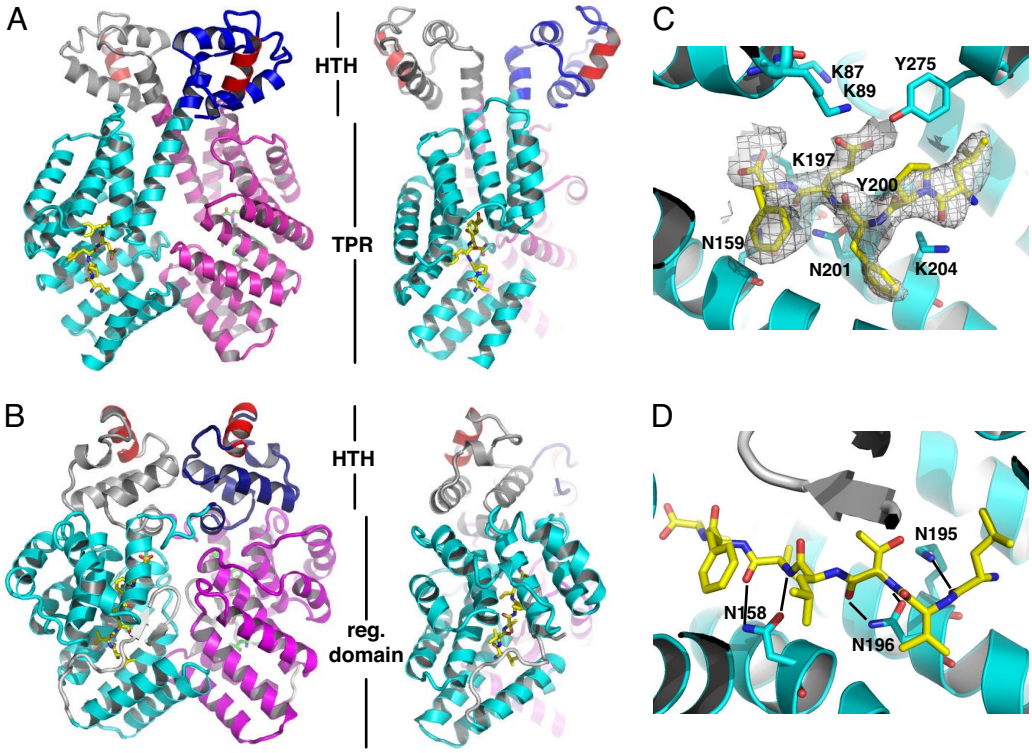

Fig. 1. Structure of PapR5:PlcR and comparison to cCF10:PrgX. Shown are ribbon presentations of PapR5:PlcR (*A*) and cCF10:PrgX (*B*) [Protein Data Bank entry 2AXZ (9)]. Chains A and B of PlcR and PrgX are colored in magenta and cyan, with their respective HTH domains in dark gray and dark blue. Helix 3 of the HTH domains that inserts into the major DNA groove is colored in red. The C-terminal extension of PrgX is colored in light gray. Ligand peptides are shown in yellow and green. *Left* and *Right* represent 90° views. (*C* and *D*) Close-up views of the peptide–protein interactions for PapR:PlcR (*C*) and cCF10:PrgX (*D*). Oligopeptides are yellow, and key residues are labeled. Unbiased $3F_o–2F_c$ electron density for PapR5 is shown in gray. Hydrogen bonds between cCF10 and PrgX key residues are indicated by black lines.

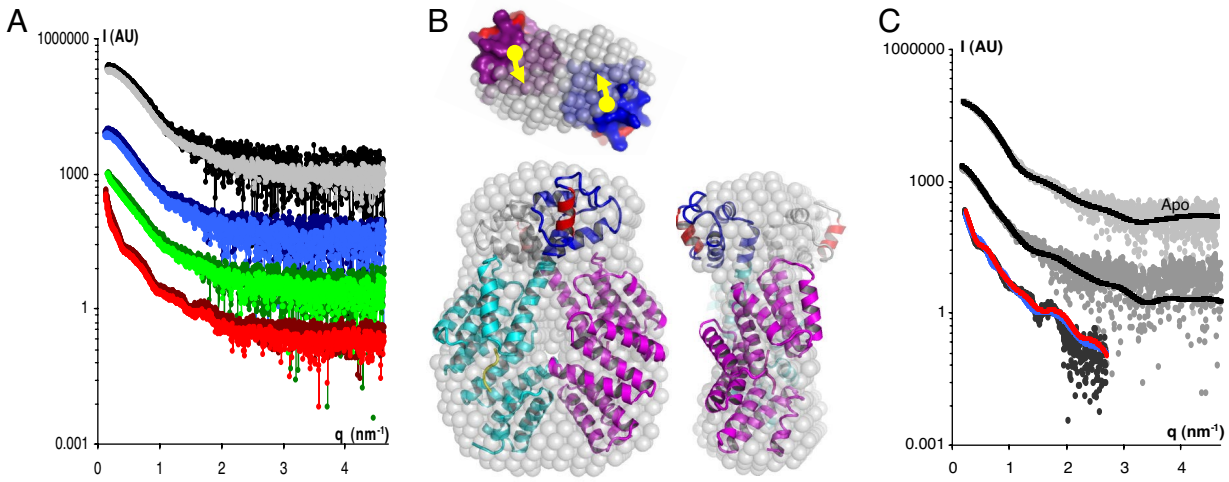

Fig. 2. SAXS data and fit of models. (*A*) SAXS pattern for apo-PlcR (black, 1.2 mg/ml; gray, 3.6 mg/ml) and PlcR in the presence of PapR5/7 at 1.2 mg/ml (blue, PapR5; light blue, PapR7), 3.0 mg/ml (green, PapR5; light green, PapR7), and 3.6 mg/ml (dark red, PapR5; red, PapR7). Intensities are in arbitrary units (AU). Curves were offset for better visibility. (*B*) Three perpendicular views of the crystallographic PapR5:PlcR dimer (color scheme as in Fig. 1*A*) fitted into the averaged SAXS *ab initio* shape obtained for apo-PlcR (gray spheres). Arrows indicate HTH movements predicted for apo-PlcR. (*C*) Fit of calculated (line) to experimental (points) SAXS curves. Top line, crystallographic PlcR dimer to apo-PlcR; middle line, crystallographic PlcR tetramer to PapR7:PlcR at 1.2 mg/ml; bottom line, crystallographic (blue) and refined (red) PapR:PlcR dodecamer to PapR5:PlcR at 3.6 mg/ml.

centrations PlcR started to precipitate) (Fig. 2*A*). Radius of gyration (Rg), Porod volume, and maximum diameter (Dm) of apo-PlcR were constant at 1.2–3.6 mg/ml and indicated that apo-PlcR was dimeric (Table 2). The crystallographic PapR5:PlcR dimer was in good agreement with the SAXS pattern and *ab initio* shape obtained for apo-PlcR, suggesting that apo-PlcR is structurally very close to the crystallized PapR5:PlcR dimer, except for a small, but probably significant, rearrangement of the HTH domains (Table 2 and Fig. 2). We next recorded SAXS data on PlcR in presence of either PapR5 or the heptapeptide ADLPFEF (PapR7), which might correspond to the physiologically more relevant peptide (L.B., S. Perchat, S.T.A., S. Zorrilla, L.S., C. Henry, M. Gohar, N.D., and D.L., unpublished data). Differently from apo-PlcR, the SAXS patterns of PapR:PlcR changed with protein concentration (Fig. 2*A*). Whereas PapR:PlcR curves at 1.2 mg/ml were not too dissimilar from those of apo-PlcR at both 1.2 and 3.6 mg/ml, this difference increased with increasing PapR:PlcR concentration. At 3.6 mg/ml, the regularly spaced ripples in the PapR:PlcR scattering curve indicated the presence of well defined supramolecular structures (Fig. 2). Already at 1.2 mg/ml, the volume, Rg, and Dm of PapR:PlcR were greater than for apo-PlcR at both 1.2 and 3.6 mg/ml and increased even further at 3.0 and 3.6 mg/ml, demonstrating that the size of the solute PapR:PlcR

Table 2. Summary of SAXS data recording and model fitting

				χ values				
Data	Rg, nm	Volumes, nm^3	Dm, nm	Dimer	Tetramer	Tetramer$_{ref}$	Dodecamer	Dodecamer$_{ref}$
Apo								
1.2 mg/ml	3.0 ± 0.2	125 ± 20/110*	9.8 ± 0.5	1.5*	5.5*	ND	ND	ND
3.6 mg/ml	3.1 ± 0.2	130 ± 20	10.0 ± 0.5					
PapR5(7)†								
1.2 mg/ml	3.7 (3.8) ± 0.2	160 (180)	12.0 (13.0) ± 1.0	2.7 (2.7)	1.6 (1.4)	1.5 (1.4)	ND	ND
3.0 mg/ml	4.1 (4.5) ± 0.5	200 (240)	15.0 (16.5) ± 2.0	2.6 (4.1)	1.7 (2.0)	1.8 (2.1)	ND	ND
3.6 mg/ml	6.4 (5.8) ± 2.0‡	720 (540)	20.5 (19.5) ± 2.0	ND	ND	ND	8.5 (8.9)§	2.4 (5.0)§
Calculated values								
Dimer	2.8	90	9.4					
Tetramer	4.1	180	14.0					
Tetramer$_{ref}$	4.1	180	13.8					
Dodecamer	7.4	540	23.0					
Dodecamer$_{ref}$	7.2	540	21.8					

Experimental Rg and Dm values were calculated by using the Guinier plot [PRIMUS (30)] and GNOM (31), respectively. Rg and Dm values of model coordinates were calculated with MOLEMAN2 (41) and do not account for a hydration shell. Model volumes were calculated by using a mean volume of 151 Å^3 per residue. χ values for the model-to-SAXS data fit were obtained by using CRYSOL (34). Volumes were determined by DAMMIN (32), except for Apo volumes, which were calculated by using Porod volumes (PRIMUS).

*Calculated for merged data.

†Values in parentheses are for PapR7.

‡Values are compromised by aggregation.

§Rigid body fit was carried out against Papr5:PlcR data.

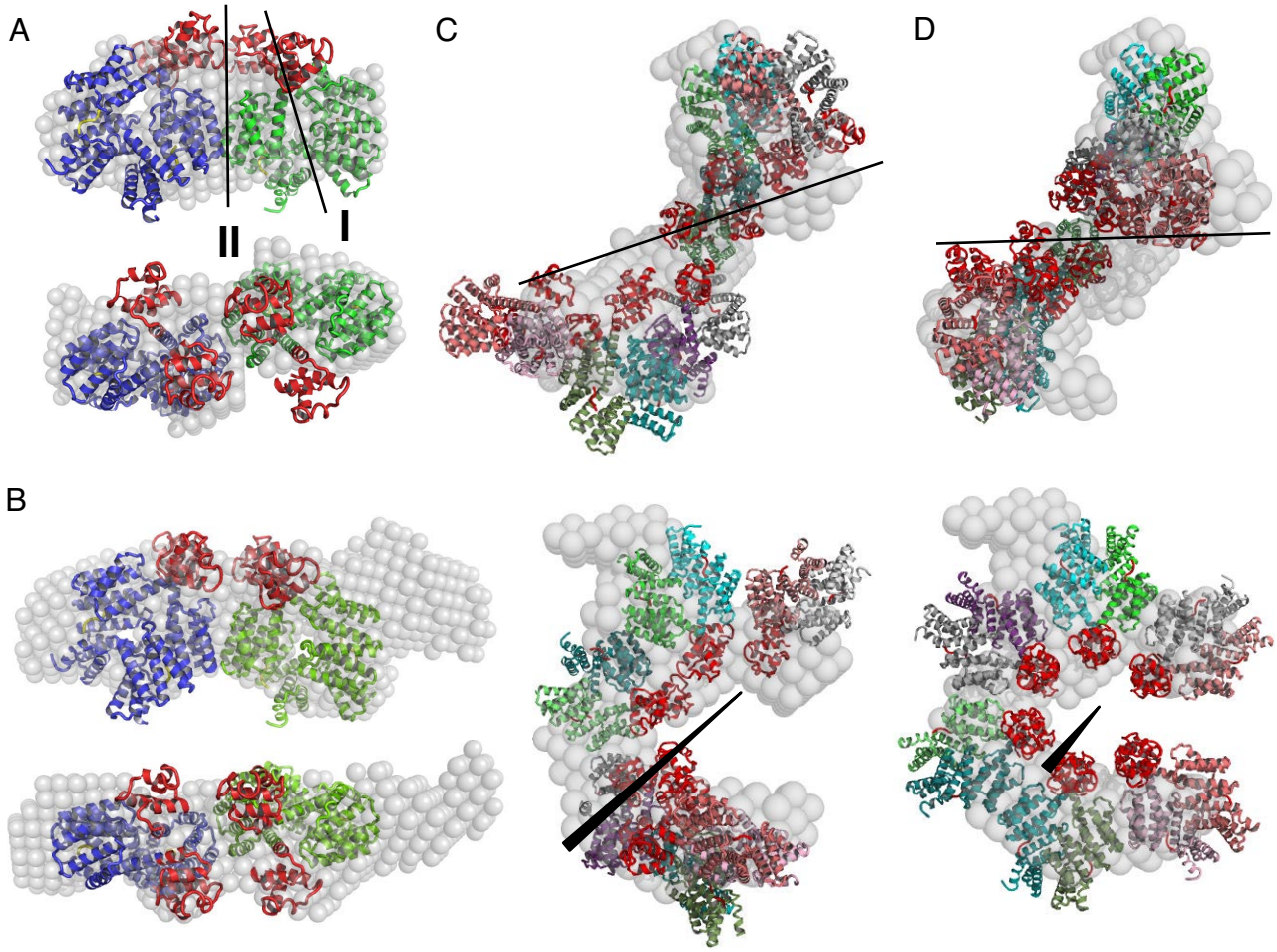

Fig. 3. PapR triggers PlcR polymerization. (*A*) Ninety-degree views of the crystallographic tetramers (ribbon representation) fitted into the *ab initio* SAXS envelope (gray) obtained for PapR:PlcR at 1.2 mg/ml. Type I and type II dimer axes are indicated. (*B*) Tetramer, obtained after rigid body refinement, superimposed onto the SAXS envelope obtained for PapR:PlcR at 3.0 mg/ml. (*C* and *D*) Ninety-degree views of SAXS envelopes (gray) obtained for data of PapR:PlcR at 3.6 mg/ml, superimposed on PlcR hexa-(dimers) taken from the crystal lattice (*C*) and after rigid body refinement (*D*). Spiral axes of models are indicated.

complex increased with concentration (Table 2). Scattering curves recorded for PapR7:PlcR and PapR5:PlcR at the same concentrations superimposed very well. Thus, both PapR7 and PapR5 triggered the same specific oligomerization of PlcR.

Because protein crystals tend to include biological oligomers, we used the PISA server (13) to search the crystal lattice for PapR5:PlcR oligomers. Apart from the dimer of the asymmetric unit (dimer type I), PISA detected only one other oligomer that was potentially biologically relevant (1,070 Å^2 of total buried solvent-accessible surface, $\Delta^iG = -3.6$ kcal/M, $P = 0.39$). This crystallographic P2 dimer (dimer type II) was formed by residues 95–144 of the TPR domain. Its interface, which is conserved only among PlcR alleles, implicates several hydrophobic residues (Y95, W99, Y119, Y120, V129, Y133, and L136) and an intramolecular antiparallel β-sheet-like structure (K128, V129, and D130), with ion pairing between K128 and D130′ (Fig. 3*A* and SI Figs. 5 and 6*B*).

The tetramer obtained by linking two type I dimers via a type II interface fitted the PapR:PlcR SAXS curves and *ab initio* shape reconstructions obtained at 1.2 and 3.0 mg/ml better than the dimer (Table 2, Fig. 3 *A* and *B*, and SI Fig. 7), implying that already at the lowest concentration tested (34 μM), tetramers were dominant over dimers. The gradual increase of Dm and Rg with protein concentration indicated a dynamic concentration-dependent equilibrium of dimers, tetramers, hexamers, and possibly higher oligomers.

The multimeric PlcR chain obtained by linking type I dimers via a type II interface follows the crystallographic $P6_1$ screw axis, forming a right-handed spiral. The shape and calculated scattering pattern of a hexamer of PlcR dimers, extracted from the crystal, displayed an approximate fit to the SAXS curves and *ab initio* shape reconstructions obtained for 3.6 mg/ml PapR:PlcR (Table 2 and Figs. 2*C* and 3*C*). A subtle rigid body refinement of the type II interface was enough to make the (dimer)–hexamer fit the data well (Table 2 and Figs. 2*C* and 3*D*). Because stringent restraints were included to keep the type II interface intact, the refinement introduced only minor changes (compare models from Fig. 3 *A* and *B*), but, propagated through the five interfaces of the (dimer)–hexamer, these sufficed to substantially improve the fit. Compared with the solution species, the type II interface may have been slightly distorted in the crystal. Indeed, nonattributed electron density was visible in the type II interface of both protomers, indicating intercalation of a molecule present in the mother liquid, possibly PEG (SI Fig. 6).

How is PapR promoting polymerization and DNA association of PlcR? Comparing the structures of cCF10-bound and apo-PrgX, we observed that pheromone recognition slightly increases the curvature of the regulatory domain (Fig. 4). The structural similarity of PlcR and PrgX, and our molecular modeling and principal component analysis [using DYNAMITE (14); data not shown], support that PapR recognition triggers a similar closure of the PlcR TPR domain. TPR opening and

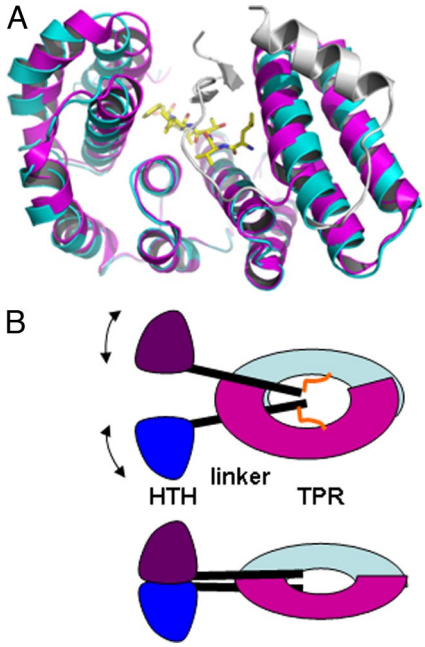

Fig. 4. Molecular effects of peptide recognition. (*A*) The curvature of the PrgX TPR-like domain increases upon autoinducer binding. Cyan, apo-PrgX (Protein Data Bank entry 2AXU); magenta, cCF10:PrgX (Protein Data Bank entry 2AXZ). The pheromone (yellow) is shown in stick representation. (*B*) Drawing illustrating how the increased TPR domain curvature in PapR:PlcR may rearrange the HTH domains. (*Lower*) apo-PlcR. (*Upper*) PapR:PlcR.

closure will result in a lever arm movement of the linker helices and hence of the HTH domains. TPR opening in absence of PapR would make both linker helices join their N termini through hydrophobic patches (solvent-exposed in our crystal), formed by residues M46, I60, I61, Y64, and I68 (Fig. 4 and SI Fig. 6). This will bring the HTH domains close together and stabilize them in their inactive orientation. The resulting HTH position, which fits well into the apo-PlcR *ab initio* SAXS envelope (Fig. 2), would sterically obstruct type II dimerization. Thus, apo-PlcR would be incapable of both DNA binding and polymerization.

TPR closure in presence of PapR would trigger the inverse lever arm movement, which opens the hydrophobic cleft between the linker helices and separates the HTH domains. In this preactivated form, corresponding to our crystal structure, polymerization is possible, and the HTH domains are mobile and predisposed to bend into a DNA-binding conformation. The HTH–HTH interface of PrgX, corresponding to a DNA-binding position, is conserved in PlcR, although solvent-exposed in our crystal (Fig. 1 and SI Fig. 5). A PrgX-like HTH interface may form in PlcR upon DNA association, concomitantly with a PrgX-like partial melting of the linker helix.

The RNPP Family of Gram-Positive Quorum Sensors. During our Psi-Blast homology searches to link PrgX and PlcR, we also retrieved many other Firmicute transcription regulators (see *SI Text*). Proteins such as TraA, RggD, MutR, and their many homologues are composed of an N-terminal HTH domain of the same subfamily as PrgX and PlcR, and a TPR-like regulatory domain with 11 predicted helices, more closely related to PrgX than to PlcR. NprR from *B. thuringiensis* and homologues from Bacilli and Clostridia possess a bona fide TPR domain with nine TPR units, TPR units 3–7 showing highest homology to PlcR (SI Fig. 5) (European Bioinformatics Institute/European Molecular Biology Laboratory database entry ALIGN_001180). Rap proteins from Bacilli are close homologues to NprR but lack the HTH domain. Accordingly, Rap proteins are not transcription regulators but control competence and sporulation through binding to cellular ligands. The interactions between Rap and cellular targets are inhibited in a population density-dependent manner by association of Rap proteins with their cognate extracellular signaling pentapeptide, CSF (2, 15).

Besides having related sequences, Rap, NprR, PlcR, and PrgX proteins also share other characteristics: (*i*) Their homologues are found only within the Gram-positive Firmicute phylum, in the classes Bacilli and Clostridia. (*ii*) They are oligopeptide quorum sensors that interact directly with their autoinducer in the responder cell, in contrast to other known quorum sensing systems (such as Com, Pln, Nis, and Spo), where the response is elicited indirectly, via binding of the secreted peptide to the extracellular part of a transmembrane histidine kinase, triggering an intracellular phosphorelay (3). (*iii*) Their signaling peptides are encoded as a precursor by a small ORF that follows directly the protein coding sequence. This precursor is cleaved to yield the active oligopeptide (15–17). Together these lines of evidence strongly suggest that all direct oligopeptide quorum sensing systems are related and derive from the same ancestor (SI Fig. 8). We propose to refer to this superfamily as the RNPP family, for Rap/NprR/PlcR/PrgX.

Discussion

Our data support that the regulatory domains of all RNPP proteins derive from a TPR domain. TPR domains, found in all kingdoms of life, are mainly used as protein–protein interaction modules. Ligand recognition is often akin to that for PlcR and PrgX. In particular, the asparagine-mediated interaction of the concave superhelix side with the peptide backbone is a conserved feature (18–20). Many TPR-containing proteins were shown or suggested to present autoinhibitory mechanisms, where a flexible tail binds back upon the convex side of the TPR domain, blocking its association with ligands (21–23). This is highly similar to the Rap-CSF system, suggesting that direct oligopeptide quorum sensing has evolved originally in *Bacillus* by acquisition of a region coding for a TPR domain and an autoinhibitory tail. By separating the TPR domain and autoinhibitory sequence into two adjacent ORFs, the Rap-CSF system was obtained, where the autoinhibitory sequence could be used as an independent extracellular signaling peptide. The long precursor of the autoinducers may be a relict of the original inhibitory tail. Accordingly, a spontaneous PlcR-PapR fusion mutant protein could activate the PlcR regulon (24). Rap proteins are likely to represent the most ancestral system because they form a highly diverse group, lack the HTH domain, still use the autoinducer to simply block binding of other ligands, and have the highest TPR "character" of RNPP proteins [TPRpred (10) indicated 100% TPR probability for Rap proteins, 86% for PlcR, and 0% for PrgX]. The association of the Rap-CSF system with a bacterial HTH domain, an arrangement unique to Firmicutes, created the NprR branch, allowing use of oligopeptide sensing in transcriptional regulation. As these proteins spread through Bacilli and Clostridia, functionally unimportant TPRs and TPR sequence characteristics were gradually lost in some members (SI Fig. 8). However, the superhelix fold and key asparagines for nonspecific peptide–backbone interactions remained conserved. Consequently, the same autoinducer recognition mechanism regulates fundamentally different processes in different bacterial genera. However, the effect of ligand binding varies and is adapted to the different tasks of RNPP proteins. Whereas autoinducer binding disrupts tetramerization of PrgX and blocks ligand binding to Rap, it triggered ordered polymerization of PlcR *in vitro*. Based on crystallographic and SAXS analysis, we propose a molecular model for PapR-dependent polymer formation. In this PapR:PlcR multimer, all HTH domains point toward the spiral axis, suggesting that polymerization and DNA binding are compatible events (Fig. 3). Favored by cooperativity with the HTH–DNA interactions, the PlcR dimer:dimer interactions might occur at much lower concentrations than those tested. Polymerization of bacterial DNA-

binding transcription regulators is not unusual and may be used to affect gene expression (for example, ref. 25). Starting from the PlcR box sequence, circular polymerization of PlcR around DNA may influence DNA topology, or displace other DNA-binding proteins, and thus impinge on gene expression.

3D structure modeling by SAXS is intrinsically underdetermined, and, at least in theory, other PlcR polymers might also fit our SAXS data. However, our dimer:dimer model is most likely, because it implies a bona fide protein–protein interface, allows fitting of PapR:PlcR SAXS patterns at all concentrations, and corresponds to the only potentially biologically relevant assembly from the crystal (obtained at the same concentration as our SAXS "spiral" species). Conversely, a PrgX-like tetramer would fit 1.2 mg/ml data reasonably ($\chi = 1.9$) but is absent in the PlcR crystal and, being point-symmetric, cannot be extended to explain the 3.6 mg/ml species. Of course, we can currently not exclude alternative roles of the PlcR dimer:dimer interface *in vivo* or the contribution of additional or alternative mechanisms such as stabilization of the C-terminal helix of PlcR by PapR.

Materials and Methods

Protein Expression and Purification. C-terminally hexahistidine-labeled *B. thuringiensis* PlcR (residues 1–293) in its native and selenomethionine substituted forms was produced and purified according to standard procedures (see *SI Text*).

Crystallographic Analysis. Native and selenomethionine proteins were kept at 4 mg/ml in 20 mM Tris (pH 8.0), 150 mM NaCl, and 2 mM DTT. The lyophilized PapR5 peptide was dissolved in 25 mM Tris (pH 8.0), 25 mM Na-phosphate (pH 8.0), and 50 mM NaCl. For crystallization, protein was mixed at a 1:5 molar ratio with PapR5. Crystals grew in hanging drops by vapor diffusion from a 1:1 mix of PapR:PlcR solution and the well solution containing 40% PEG 200, 100 mM Mes (pH 6.0–6.5). Data were recorded at 100 K on flash-cooled crystals, at beamline ID29 of the European Synchrotron Radiation Facility (Grenoble, France), at $\lambda = 0.976$ and 0.979 Å for native and selenomethionine crystals, respectively. Data were integrated and scaled by using MOSFLM and SCALA from the CCP4 program suite (26). Phases from single-wavelength anomalous diffraction were used for initial model building [COOT (27)]. This initial model was refined against 2.6-Å native data by using TLS [REFMAC (28)] (Table 1). PapR and HTH domains were built in $3F_o–2F_c$ maps [CNS (29)] calculated before PapR and HTH were included in the model. For details see *SI Text*. Coordinates and structure factors have been deposited in the Protein Data Bank under ID code 2QFC.

SAXS. Data were collected at beamline X33, at Deutsches Elektronen-Synchrotron, European Molecular Biology Laboratory (Hamburg, Germany), at 10°C, using a wavelength of $\lambda = 1.5$ Å. Samples were kept in 20 mM Tris (pH 8.0), 300 mM NaCl, and 2 mM DTT. For the PapR:PlcR complex, samples were supplemented with 500 μM PapR5 or PapR7. Data analysis, *ab initio* shape calculations, and rigid body refinement were performed by using PRIMUS, GNOM, DAMMIN, GASBOR, CRYSOL, DAMAVER, and SASREF (30–36). For details, see *SI Text*.

Phylogenetic and Sequence Analysis. Sequence searches were performed with Psi-BLAST (12) using default parameters and five or fewer iterations. The BioInfoBank metaserver (37) was used for gene threading and secondary structure predictions. Structure-based sequence alignments were established by using VITO (38). Sequence alignments were visualized with JalView using the Blosum62 coloring scheme. From these alignments, phylogenetic trees were established by using BIONJ (39) and PHYLIP (40). The alignment of SI Fig. 5 has been deposited at the European Bioinformatics Institute/European Molecular Biology Laboratory database (accession no. ALIGN_001180).

We thank D. Svergun and his colleagues for assistance with SAXS data recording and analysis at the X33 beamline at European Molecular Biology Laboratory/Deutsches Elektronen-Synchrotron. We thank X. Thiebaut for assistance with data recording at European Synchrotron Radiation Facility beamline ID29. We thank A. Chavanieu and J.-F. Guichou for PapR synthesis, C. Royer for critical reading, and G. Labesse for help with bioinformatics. We acknowledge support from European Community–Research Infrastructure Action under the Sixth Framework Program (Grant RII3/CT/2004/5060008) for access to the European Molecular Biology Laboratory/Deutsches Elektronen-Synchrotron and support from the Institut National de la Recherche Agronomique and from the Agence Nationale de la Recherche (Grant PNRA 013-04).

1. Miller MB, Bassler BL (2001) *Annu Rev Microbiol* 55:165–199.
2. Waters CM, Bassler BL (2005) *Annu Rev Cell Dev Biol* 21:319–346.
3. Dunny GM, Leonard BA (1997) *Annu Rev Microbiol* 51:527–564.
4. Lereclus D, Agaisse H, Gominet M, Salamitou S, Sanchis V (1996) *J Bacteriol* 178:2749–2756.
5. Schnepf E, Crickmore N, Van Rie J, Lereclus D, Baum J, Feitelson J, Zeigler DR, Dean DH (1998) *Microbiol Mol Biol Rev* 62:775–806.
6. Rasko DA, Altherr MR, Han CS, Ravel J (2005) *FEMS Microbiol Rev* 29:303–329.
7. Dixon TC, Meselson M, Guillemin J, Hanna PC (1999) *N Engl J Med* 341:815–826.
8. Slamti L, Lereclus D (2002) *EMBO J* 21:4550–4559.
9. Shi K, Brown CK, Gu ZY, Kozlowicz BK, Dunny GM, Ohlendorf DH, Earhart CA (2005) *Proc Natl Acad Sci USA* 102:18596–18601.
10. Karpenahalli MR, Lupas AN, Soding J (2007) *BMC Bioinformatics* 8:2.
11. Holm L, Sander C (1995) *Trends Biochem Sci* 20:478–480.
12. Altschul SF, Madden TL, Schaffer AA, Zhang J, Zhang Z, Miller W, Lipman DJ (1997) *Nucleic Acids Res* 25:3389–3402.
13. Krissinel E, Henrick K (2007) *J Mol Biol* 372:774–797.
14. Barrett CP, Hall BA, Noble ME (2004) *Acta Crystallogr D* 60:2280–2287.
15. Perego M, Brannigan JA (2001) *Peptides* 22:1541–1547.
16. Core L, Perego M (2003) *Mol Microbiol* 49:1509–1522.
17. Hirt H, Manias DA, Bryan EM, Klein JR, Marklund JK, Staddon JH, Paustian ML, Kapur V, Dunny GM (2005) *J Bacteriol* 187:1044–1054.
18. D'Andrea LD, Regan L (2003) *Trends Biochem Sci* 28:655–662.
19. Jinek M, Rehwinkel J, Lazarus BD, Izaurralde E, Hanover JA, Conti E (2004) *Nat Struct Mol Biol* 11:1001–1007.
20. Kim K, Oh J, Han D, Kim EE, Lee B, Kim Y (2006) *Biochem Biophys Res Commun* 340:1028–1038.
21. Grizot S, Fieschi F, Dagher MC, Pebay-Peyroula E (2001) *J Biol Chem* 276:21627–21631.
22. Yang J, Roe SM, Cliff MJ, Williams MA, Ladbury JE, Cohen PT, Barford D (2005) *EMBO J* 24:1–10.
23. Du Q, Macara IG (2004) *Cell* 119:503–516.
24. Pomerantsev AP, Pomerantseva OM, Leppla SH (2004) *Infect Immun* 72:5814–5823.
25. Bouffartigues E, Buckle M, Badaut C, Travers A, Rimsky S (2007) *Nat Struct Mol Biol* 14:441–448.
26. CCP4 (1994) *Acta Crystallogr D* 50:760–763.
27. Emsley P, Cowtan K (2004) *Acta Crystallogr D* 60:2126–2132.
28. Murshudov GN, Vagin AA, Dodson EJ (1997) *Acta Crystallogr D* 53:240–255.
29. Brunger AT, Adams PD, Clore GM, DeLano WL, Gros P, Grosse-Kunstleve RW, Jiang JS, Kuszewski J, Nilges M, Pannu NS, *et al.* (1998) *Acta Crystallogr D* 54:905–921.
30. Konarev PV, Vladimir VV, Sokolova AV, Koch MJ, Svergun DI (2003) *J Appl Crystallogr* 36:1277–1282.
31. Svergun DI (1992) *J Appl Crystallogr* 25:495–503.
32. Svergun DI (1999) *Biophys J* 76:2879–2886.
33. Svergun DI, Petoukhov MV, Koch MH (2001) *Biophys J* 80:2946–2953.
34. Svergun DI, Barberato C, Koch MHJ (1995) *J Appl Crystallogr* 28:768–773.
35. Volkov VV, Svergun DI (2003) *J Appl Crystallogr* 36:860–864.
36. Petoukhov MV, Svergun DI (2005) *Biophys J* 89:1237–1250.
37. Ginalski K, Elofsson A, Fischer D, Rychlewski L (2003) *Bioinformatics* 19:1015–1018.
38. Catherinot V, Labesse G (2004) *Bioinformatics* 20:3694–3696.
39. Gascuel O (1997) *Mol Biol Evol* 14:685–695.
40. Felsenstein J (1997) *Syst Biol* 46:101–111.
41. Kleywegt GJ, Harris MR, Zou JY, Taylor TC, Wahlby A, Jones TA (2004) *Acta Crystallogr D* 60:2240–2249.